

# Compact string reactor for autothermal hydrogen production

C. Horny, A. Renken, L. Kiwi-Minsker\*

*École Polytechnique Fédérale de Lausanne, EPFL-LGRC, CH-1015 Lausanne, Switzerland*

Available online 22 August 2006

## Abstract

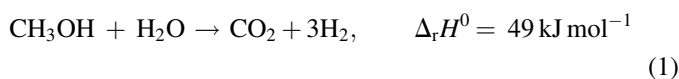
This study addresses the development of a compact reactor for oxidative steam-reforming of methanol (OSRM) to produce hydrogen in autothermal mode for fuel cells. The string reactor uses catalytically active brass wires with a diameter of 500  $\mu\text{m}$  placed in parallel into a tube. The micro-channels in the reactor for gases are formed between the wires presenting hydrodynamics similar to the one in multi-channel micro-reactors. Due to the high thermal conductivity of brass, the heat generated during methanol oxidation at the reactor entrance is transferred to the zone of the endothermic steam-reforming. The catalysts are prepared by Al-alloy formation on the surface of the brass wires followed by the partial leaching of Al. The catalyst presents a porous layer with the morphology of Raney metals and the chemical composition consistent with the Cu/Zn/Al-mixed oxide. The catalyst surface was additionally modified by incorporating chromium leading to Cr/Cu-spinel. This decreases the degree of the reduction of copper oxide and sintering leading to a stable catalyst. The catalyst was tested in OSRM showing high activity and selectivity to carbon dioxide and hydrogen. The string reactor presents nearly isothermal profile since the temperatures gradient within the reactor length is about 3 K. Micro-structured string reactor presents a short start-up and a fast transient behavior showing a rapid temperature change when adjusting the oxygen amount introduced into the reactor.

© 2006 Elsevier B.V. All rights reserved.

*Keywords:* Autothermal hydrogen production; Methanol; Oxidative steam-reforming; Brass-wire catalysts; Micro-structured reactor; Hot-spot; Raney metal

## 1. Introduction

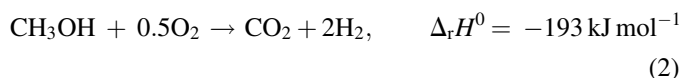
Methanol is considered for “automotive” fuel cells as hydrogen source due its safe handling, low cost and high storage density. Moreover, it can be produced from biological, i.e. renewable sources [1]. Between different reactions, steam-reforming (SR) gives the highest hydrogen concentration (up to 75%):



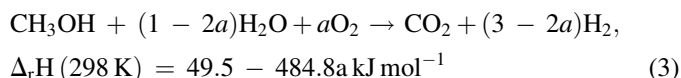
The amount of CO generated along  $\text{CO}_2$  according the reaction (1), is low. This is important since it acts as a poison for fuel cells. The accepted levels of CO are between 10 and 100 ppm [2,3].

The main disadvantage of SR is its endothermicity requiring external heating, which makes short start-up and fast transient behavior difficult to achieve [4].

The exothermic partial oxidation of methanol (POX) can be used for fast dynamic in reforming systems:



But the formation of hot-spots in the catalytic bed is the main drawback: it leads to catalyst sintering resulting in the activity loss [5]. Combined SR and POX is known as oxidative steam-reforming of methanol (OSRM) which gives fast dynamics and generates high hydrogen concentrations:



Reactors for this process operate autothermally, i.e. it does not require any external heating or cooling once the operational temperature is reached. For fast transient response, the methanol/oxygen ratio can be varied as in the case of the Hot-Spot<sup>®</sup> reformer [6].

OSRM takes place over copper/zinc/alumina (CZA) catalysts with high activity and selectivity to  $\text{CO}_2$  and  $\text{H}_2$ . Optimum feed composition was reported having oxygen to methanol and water to methanol ratios of 0.2–0.3 and 1.3–1.6,

\* Corresponding author. Fax: +41 21 693 3190.

E-mail address: [liubov.kiwi-minsker@epfl.ch](mailto:liubov.kiwi-minsker@epfl.ch) (L. Kiwi-Minsker).

respectively [7–9]. The excess steam serves to reduce CO content by water–gas shift reaction:



## 2. Reactor concept

The main difficulty in carrying out OSRM is due to the fast methanol oxidation compared to the steam-reforming. As a consequence, heat is generated mostly at the reactor entrance, whereas the heat consumption occurs in the middle and rear of the reactor. In conventional reactors with randomly packed catalytic beds, low axial and radial heat conductivity leads to substantial axial temperature profiles. A hot-spot at the reactor entrance and a “cold-spot” in the second part of the reactor were observed [10]. A high temperature damages the catalyst. On the other hand, a low temperature decreases the rate of the reforming reaction. Therefore, temperature control in the reactor is crucial for an efficient and stable reactor performance.

Metal-based catalysts with high thermal conductivity allow combining exothermic combustion of methanol and endothermic steam-reforming. The beneficial effect of improved heat transfer was demonstrated for the OSRM using either a conductive material [11], or channel micro-geometry of a monolith [12].

In the present study, a compact String reactor<sup>®</sup> is applied for OSRM [13–15]. The reactor consists of a tube with a diameter in the centimeter range where thin metallic catalyst wires are introduced with diameters of 500  $\mu\text{m}$  (Fig. 1). The reacting gases flow between the wires. The string reactor presents a flow hydrodynamics similar to multi-channel micro-reactors [13,15] and ensures laminar flow, narrow residence time distribution and low pressure drop through the catalytic bed. Brass wires with high heat conductivity (118 W/(m K)) were chosen as catalyst due to their chemical composition (alloy of Cu and Zn) close to the conventional CuZnAl-mixed oxide catalyzing the OSRM.

## 3. Experimental

### 3.1. Catalyst preparation

The brass-wires CuZn37 (from Goodfellow) containing 37 wt.% of zinc were used as catalyst. The specific surface area

(SSA) of the wires corresponds to their geometric surface per volume and therefore, they did not show any catalytic activity [15]. To obtain metal wires with high SSA, a thin Cu/Zn/Al alloy is formed on the wire surface. Then, aluminium is leached out resulting in a thin porous layer with a morphology similar to that of Raney metals [16]. Aluminium leaching is carried out either in an acid or a basic solution. The acid leaching uses boiling HCl aqueous solution (3.7 wt.%) during 20 min. The catalyst treated by this acid leaching is named CZA.

The leaching by basic medium is carried out simultaneously with a metal doping by two different methods: impregnation (of chromium) or precipitation (of chromium, zirconium or cerium). Leaching of aluminium and impregnation with chromium were performed using  $(\text{NH}_4)_2\text{Cr}_2\text{O}_7$  (0.004 M) in an aqueous solution of NaOH 6.1 M at 273 K during 72 h. The resulting catalyst is CZACr/i. Metal precipitation together with aluminium leaching is carried out by using nitrate metals ( $\text{M}^{x+}(\text{NO}_3)_x$ ) 0.5 M in an aqueous solution of  $\text{Na}_2\text{CO}_3$  0.1 M at 333 K during 30 min. When adding Cr, Zr or Ce, the catalysts were named after the dopant as CZACr/p, CZAZr/p and CZACe/p. After rinsing in water, catalysts were calcined in air at 723 K for 2 h, and before testing reduced by 10%  $\text{H}_2$  in Ar at 523 K during 2 h in the reactor.

### 3.2. Characterization of the catalysts

The specific surface area of the samples was measured by nitrogen adsorption using a Sorptomatic 1990 (Carlo Erba) instrument and calculated applying BET method.

SEM images were obtained with a SEM JSM 6300 (JEOL USA, Inc., Peabody, MA, USA) apparatus.

Temperature-programmed reduction (TPR) and oxidation (TPO) were carried out in a Micromeritics AutoChem 2910 apparatus by passing, respectively, the flows (20 ml/min (STP)) of 4 vol.%  $\text{H}_2$  in He and 2 vol.%  $\text{O}_2$  in He through the sample (ca. 150 mg). The temperature was increased from room temperature to 1073 K at a rate of 10 K/min. The outlet concentrations were monitored by a mass spectrometer (Thermostar 200, Pfeiffer Vacuum) to obtain TPO and TPR profiles.

X-ray photoelectron spectra (XPS) was performed with a Kratos AXIS Ultra, UK. The binding energies of Cu 2p were referenced to the C 1s peak at 285.2 eV, giving binding energies with  $\pm 0.2$  eV experimental error.

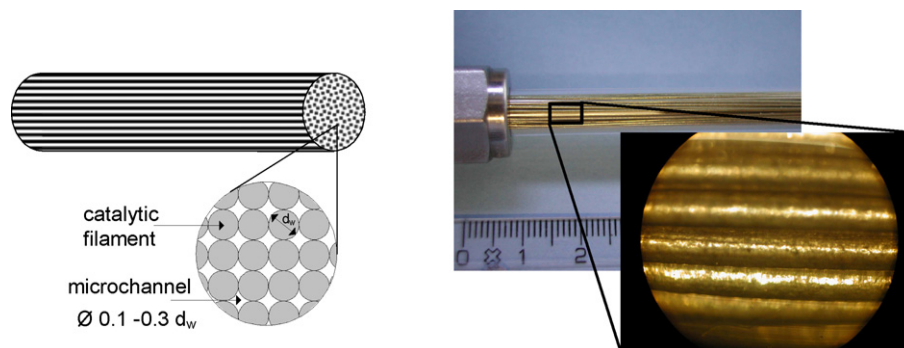


Fig. 1. Schematic presentation and photograph of the compact string-reactor.

### 3.3. Experimental set-up and reaction conditions

The reactions were performed at  $1.32 \times 10^5$  Pa pressure and temperatures between 473 and 573 K. The ratios of water to methanol and oxygen to methanol were 1.0 and 0.12, respectively, with argon as diluting gas.

A tubular glass reactor (inner diameter: 9 mm, length: 110 mm) was filled with 217 catalytic active metal rods (39.4 g) and placed in a furnace. In the middle of the catalytic bed, a thermocouple with a stainless steel sheath was inserted. The thermocouple with the same dimension as the metal rod could be displaced axially to measure the axial temperature profile. Pre-mixed water–methanol was fed to a vaporizer (Bronkhorst High-Tech B.V.) heated at 398 K with argon as carrier gas. Gas and liquid flows were adjusted by Bronkhorst mass flow controllers. The whole installation was maintained at 423 K in order to avoid condensation in the tubing. The feed and product gases were analyzed by on-line gas chromatography (Hewlett Packard, HP 6890, capillary column: Supelco Carboxen 1010) with a thermal conductivity detector.

## 4. Results and discussion

### 4.1. Influence of chemical composition and preparation method on catalyst performance

Oxidative steam-reforming of methanol was carried out over brass-based catalysts, leached in an acidic solution (CZA) or doped and leached in a basic solution. The modification of the catalyst was performed by impregnation or by precipitation (Cr, Zr, Ce). Fig. 2 shows methanol conversion and hydrogen production for different catalysts under the same conditions. Those prepared by the precipitation, demonstrated very low activity with methanol conversion of 10–18% and hydrogen production of less than 0.2 mL/(g<sub>cat</sub> min). At the same time formaldehyde and formic acid were detected. These secondary products are formed by dehydrogenation or partial oxidation of methanol in line with the results reported in literature [17–19].

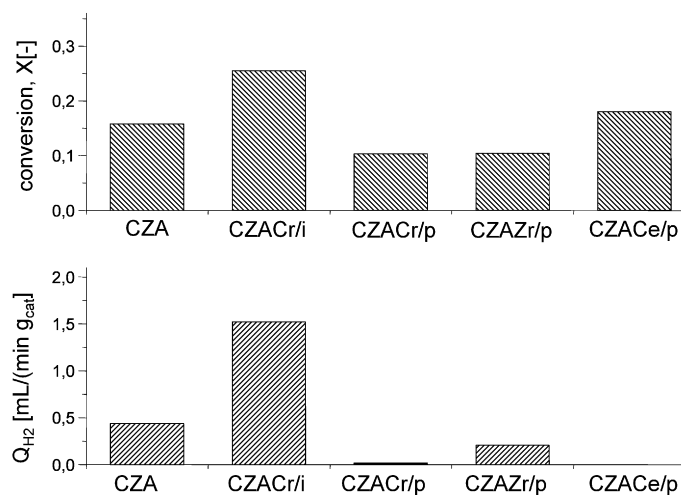


Fig. 2. Oxidative steam-reforming of methanol: influence of additives and preparation methods on hydrogen production after 1 h of reaction.  $T = 537$  K;  $W/F = 0.3$  kg<sub>cat</sub> s/mmol; total flow = 100 mL/min.

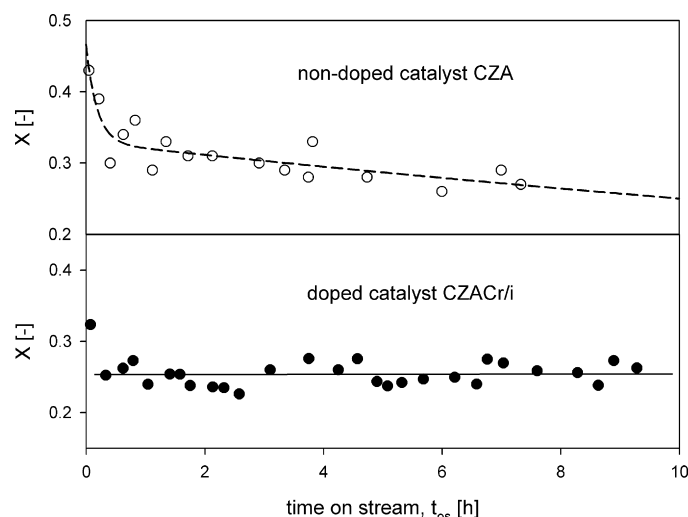


Fig. 3. Oxidative steam-reforming of methanol. Stability of the non-doped catalyst (CZA) and the Cr-doped catalyst (CZACr/i).  $T = 535$  K;  $W/F = 0.3$  kg<sub>cat</sub> s/mmol; total flow = 100 mL/min.

Impregnation of the Raney catalysts with chromium is known to improve the activity/selectivity of Cu-based catalyst [20–22]. The experimental results obtained in this study and showed in Fig. 2 demonstrate the higher production of hydrogen of the catalyst doped with chromium by impregnation (CZACr/i). The higher stability of this catalyst is demonstrated in Fig. 3, where the methanol conversion is plotted as a function of time. Therefore, the CZACr/i catalyst was used for further studies.

Non-treated brass rods gave no measurable methanol conversion under the chosen reaction conditions.

### 4.2. Catalyst characterization

#### 4.2.1. BET surface area

Surface areas and methanol conversions of the non-doped and doped catalysts were measured before and after reaction and are reported in Table 1. In view of these results, the loss of activity during oxidative steam-reforming of methanol can be related to the loss of specific surface area. Indeed, because of the low Hüttig temperature, copper is highly sensitive to thermal sintering [23]. This process reduces the SSA decreasing the catalytic activity [23–25].

#### 4.2.2. SEM images

The surface porosity is clearly seen by SEM images. Fig. 4 shows the surface morphology of the wires of CZA and

Table 1  
BET surface area and methanol conversion before and after reaction of the non-doped (CZA) and the Cr-doped (CZACr/i) catalysts

Catalyst	Surface area (m <sup>2</sup> /g)			Methanol conversion		
	Initial	Final	Ratio final/initial	Initial	Final	Ratio final/initial
CZA	23.0	14.9	0.648	0.430	0.270	0.628
CZACr/i	19.0	15.3	0.805	0.324	0.253	0.781

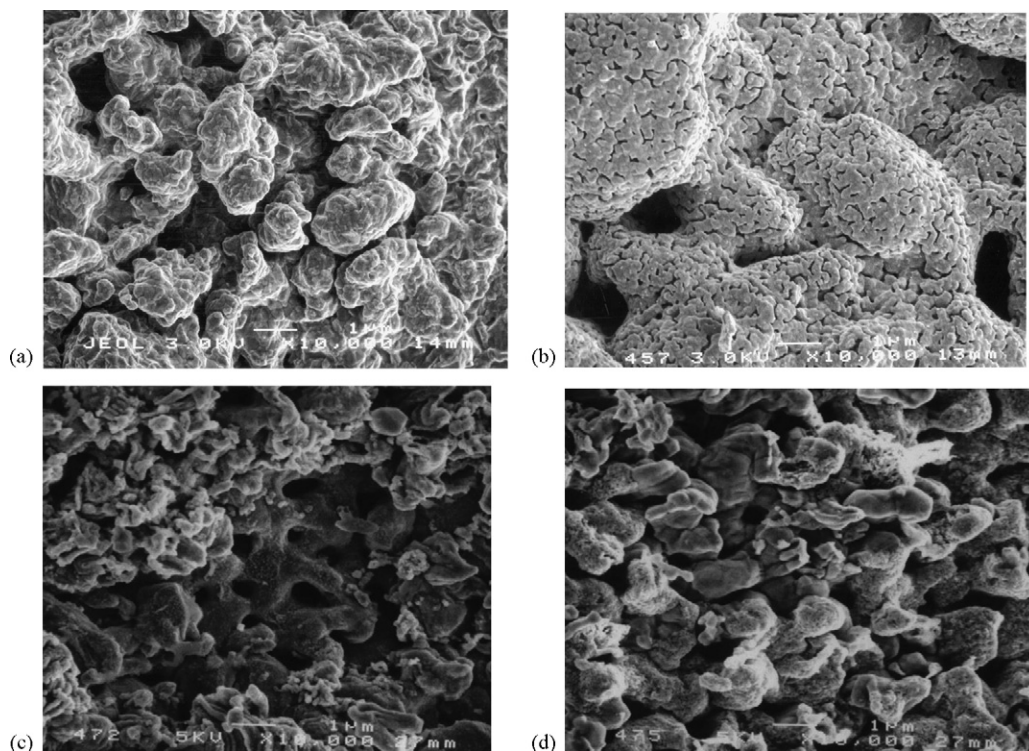


Fig. 4. SEM image of the surface: CZA after calcination (a) and after reduction (b); CZACr/i after calcination (c) and after reduction (d).

CZACr/i after calcination and after reduction. The surface of the non-doped catalyst has been modified during reduction, whereas the one of the Cr-doped catalyst remain unchanged.

#### 4.2.3. XPS

Photoelectron spectroscopy was used to study the chemical state of the elements and their relative abundance at the catalyst surfaces. The binding energies of Cu 2p for CZA and CZACr/i catalysts after oxidation and after reduction are summarized in Table 2 and the spectra are displayed in Figs. 5 and 6. For the non-doped catalyst, the Cu 2p profile changes dramatically upon H<sub>2</sub>-reduction. The calcined sample (Fig. 5(a)) displays a unique Cu peak at approximately 934 eV, which is characteristic of Cu<sup>2+</sup> in CuO [26]. In addition, the satellite peak at ~943 eV indicates Cu<sup>2+</sup> ions, since it is considered as a charge transfer of ligand electrons to unfilled 3d orbital [27,28]. The

decrease of the satellite peak and the simultaneous shift of the principal Cu 2p peak towards lower binding energy upon H<sub>2</sub>-reduction (Fig. 5(b)) suggest that the copper species are transformed to Cu<sup>+</sup> or Cu<sup>0</sup> (70%) [29]. The Cu 2p peak presents

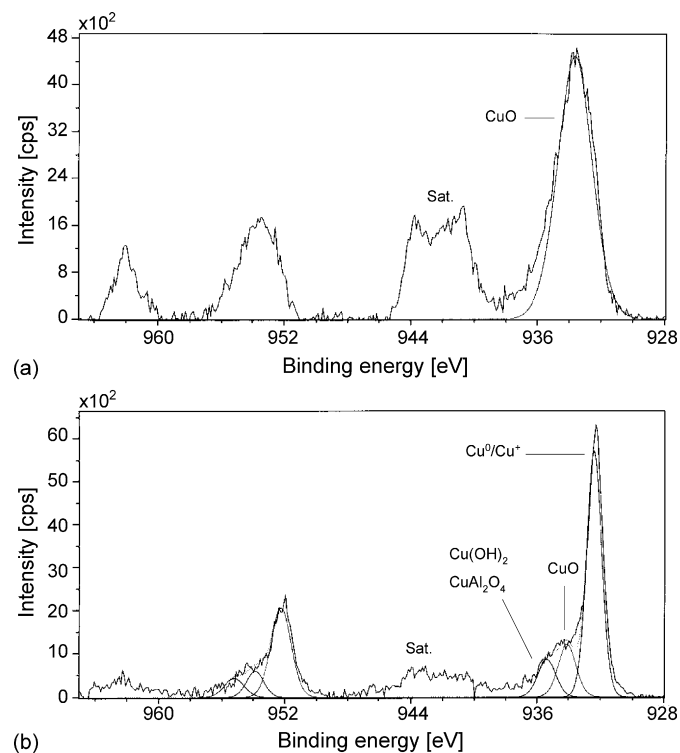


Fig. 5. Cu 2p X-ray photoelectron spectra of the non-doped catalyst (CZA) after calcination (a) and after reduction (b).

Table 2  
Binding energies values of Cu 2p (eV) for CZA and CZACr/i catalysts after oxidation and after reduction

After calcination	After reduction
CZA	
933.7 (100)	932.5 (70.0)
	934.1 (17.0)
	935.4 (13.0)
CZACr/i	
934.0 (5.8)	932.8 (11.0)
935.0 (94.2)	934.1 (39.0)
	935.3 (50.0)

Values in parenthesis are peak percentages.

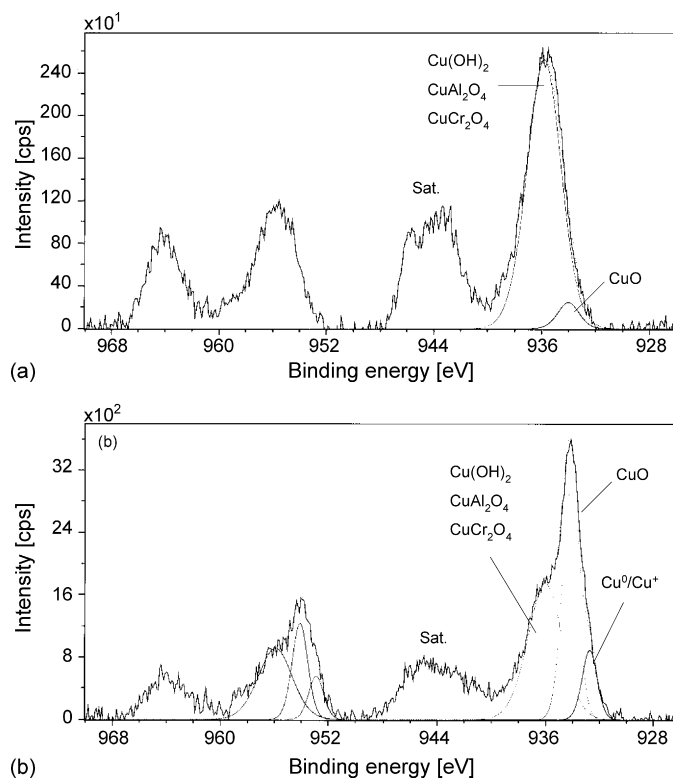


Fig. 6. Cu 2p X-ray photoelectron spectra of the Cr-doped catalyst (CZACr/i) after calcination (a) and after reduction (b).

a higher energy shoulder, which can be deconvoluted in two components: at 934.0 eV assigned to CuO (17%), and above 935.0 eV related to  $\text{Cu}^{2+}$  ions interacting with the hydroxyl groups of ZnO or in a  $\text{CuAl}_2\text{O}_4$  spinel-type compound (13%) [27,30].

From Fig. 6(a), the calcined Cr-doped catalyst shows a unique large peak which consists of more than one contributions. The main part at 935 eV is related to  $\text{Cu}^{2+}$  ions in the form of  $\text{Cu}(\text{OH})_2$  or in the environment of a  $\text{CuAl}_2\text{O}_4$  or  $\text{CuCr}_2\text{O}_4$ . A small contribution (6%) is due to CuO at 934.0 eV. The satellite peak at 943 eV is again observed, confirming the presence of  $\text{Cu}^{2+}$  ions. The reduced catalyst (Fig. 6(b)) does not show important modifications: contribution of  $\text{Cu}^{2+}$  in the form of CuO is bigger (~40%) and the surface presents a low content of copper as  $\text{Cu}^+$  or  $\text{Cu}^0$ .

The two catalysts – with and without chromium – have different behaviors towards reduction: the CZA catalyst is easily reduced to  $\text{Cu}^+$  or  $\text{Cu}^0$  whereas the CZACr shows mainly the oxidized copper in form of the spinels. These observations agree with work reported by other groups [26–28,30–32].

#### 4.2.4. TPR–TPO

The calcined and reduced catalysts were subjected to TPR and TPO measurements to provide information about the copper reducibility.

The TPR profiles of the calcined catalysts are shown in Fig. 7. The non-doped catalyst shows two broad peaks at 623 and 693 K whereas the doped catalyst presents a unique small peak at 593 K. The presence of the doublet is explained either

by the two steps reduction of copper [31,33] (Eq. (5)) or by the reduction of copper interacting with zinc



Moreover, it has been shown that a broad peak is characteristic of a strong interaction between two elements Cu and Zn [31] and that copper oxide in the presence of zinc is reduced at lower temperatures than copper oxide alone [33–35]. As a result, the peak of the CZACr/i catalyst corresponds to the reduction of copper interacting with Zn or Cr. The hydrogen

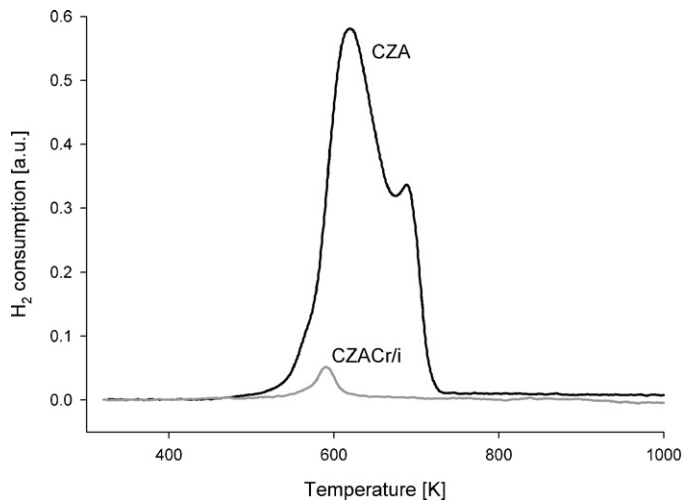


Fig. 7. TPR profiles of the calcined catalysts.

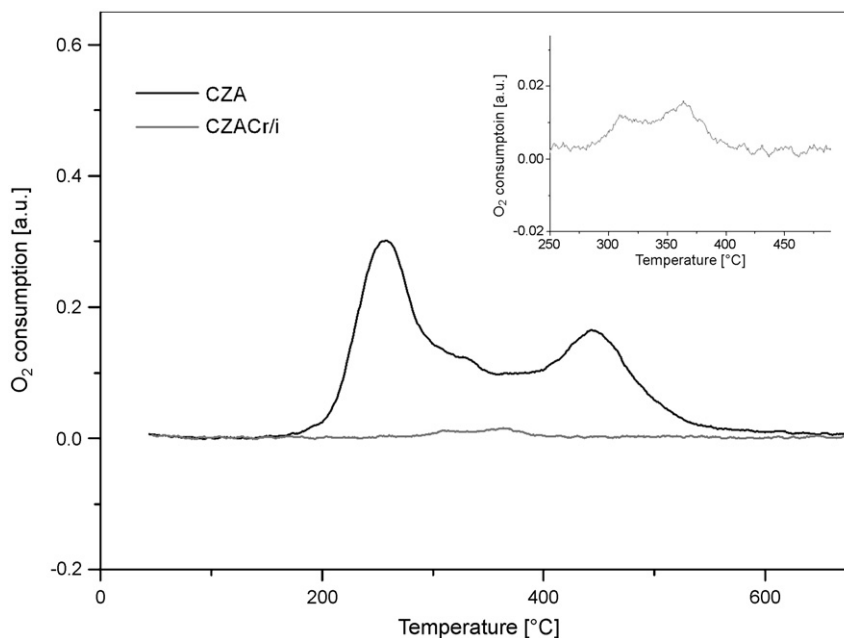


Fig. 8. TPO profiles of the reduced catalysts (inset: CZACr/i).

consumption of the doped catalyst is low because a spinel structure is difficult to reduce [36].

The TPO profiles of the reduced catalysts are shown in Fig. 8. The non-doped catalyst shows a multi-peak profile [30] and is attributed to the reverse reaction of Eq. (5). On the contrary, the doped catalyst is characterized by low oxygen consumption indicating that the Cr-doped catalyst is in the oxidized state.

#### 4.3. Catalytic activity

A series of experiments was carried out by varying the contact time, i.e. changing the total flow rate while keeping methanol and oxygen concentration constant at 13 and 12%, respectively. The effects of contact time and temperature on the methanol conversion and CO-selectivity (Eq. (6)) are found and presented in Fig. 9. The experimental error is estimated to be  $\pm 5\%$ .

$$S_{\text{CO}} = \frac{C_{\text{CO}}}{C_{\text{CO}} + C_{\text{CO}_2}} \quad (6)$$

At longer contact times and higher temperatures the increased conversions were observed. Likewise, the CO-levels increase with increasing contact time and temperature.

Different reaction schemes have been suggested for the generation of CO by-product. Santacesaria and Carra [37] and Amphlett et al. [38] proposed a sequence of decomposition—water–gas shift (WGS) reaction: CO is a primary product subsequently converted into  $\text{CO}_2$  in the WGS reaction accompanied by  $\text{H}_2$  production. Parallel reactions between methanol SR and decomposition have been reported [39], with the CO/ $\text{CO}_2$  ratio adjusted by the WGS equilibrium.

A direct mechanism was proposed initially by Takahashi et al. [40]: the methylformate reaction route where no WGS is involved. In this case methanol dehydrogenation (Eq. (7)) to

methylformate takes place, followed by the hydrolysis to formic acid (Eq. (8)) which subsequently decomposes into  $\text{CO}_2$  and  $\text{H}_2$  (Eq. (9)). CO is proposed to be formed as a secondary product by the reverse WGS reaction (Eq. (10)).

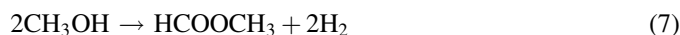


Fig. 10 shows the CO-selectivity plotted against methanol conversion and compared to the equilibrium selectivity calculated for the water–gas shift reaction (Eq. (4)). Thermodynamic

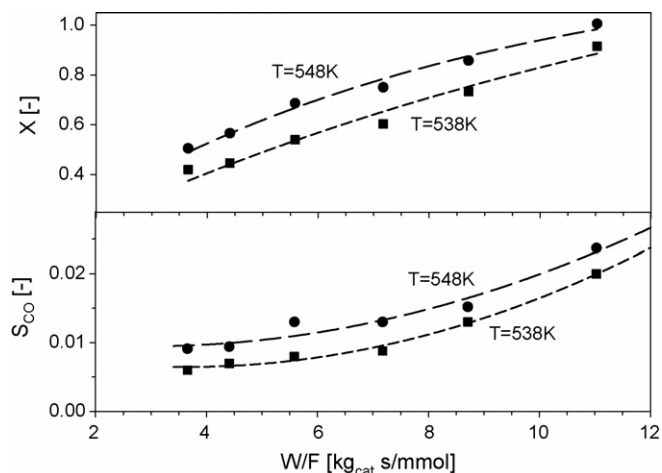


Fig. 9. Methanol conversion and CO-selectivity vs. contact time for oxidative steam-reforming over CZACr/i at 538 and 548 K. Pressure 0.13 MPa, methanol: 13 mol%, oxygen: 12 mol%, water: 13%, rest: argon.

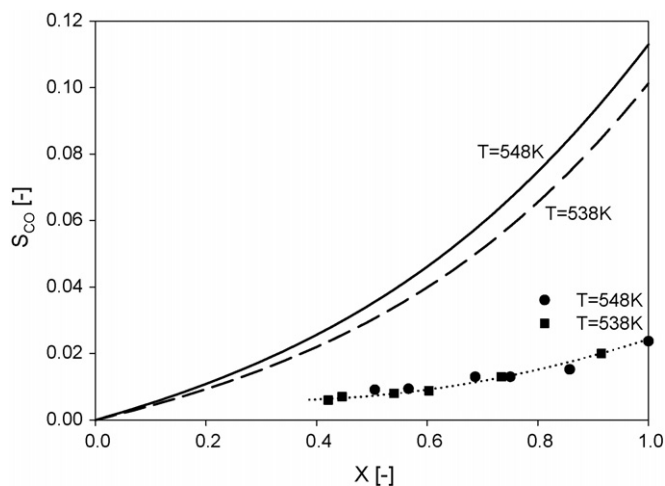


Fig. 10. CO<sub>2</sub>-selectivity as a function of methanol conversion (CZACr/i). Equilibrium (lines) and measured values (points) at 538 K and 548 K.

data were taken from Reid et al. [41]. The product composition is seen to be far from equilibrium: CO-levels are well below those predicted by equilibrium for the WGS reaction. This result suggests that carbon monoxide is not formed as a primary product of methanol decomposition, but as a secondary product in a consecutive reaction. Similar results are reported in the literature confirming the above reaction mechanism [5,8,42–44]. WGS can be neglected under the conditions of the SR reaction [45] although copper-zinc-alumina catalysts are known to be active for low temperature WGS reaction [46,47]. The lack of CO formation was explained by the surface blocking by the strongly adsorbed methanol and methylformate [45]. The concentration of carbon monoxide was about 2500 ppm at complete conversion at 548 K. This value is above the allowed limit, but it is adequate for the separation in a Pd membrane or by preferential oxidation [1,6].

#### 4.4. Thermal behavior of the string reactor

Oxidative steam-reforming was carried out over CZACr in the string reactor of 110 mm length. The reactor temperature was measured in the center of the reactor at different axial positions.

##### 4.4.1. Reactor dynamics during the start-up

The transient thermal behavior during a start-up of the reactor for OSRM was studied by monitoring the temperatures at four axial positions: 8, 31, 62 and 105 mm and are shown in Fig. 11 as function of time. The initial temperature was 535 K and corresponded to the wall temperature of the reactor. At time  $t = 0$ , the inert gas (Ar) was replaced by the reaction mixture (methanol 16.5%, water 16.5% and oxygen 2% in Ar). The temperature at the reactor entrance (8 mm) increased rapidly within the first 10 min and reached steady state after ~20 min. The steep temperature rise is due to the fast exothermic methanol oxidation, which takes place in the first part of the reactor. With increasing distance from the reactor

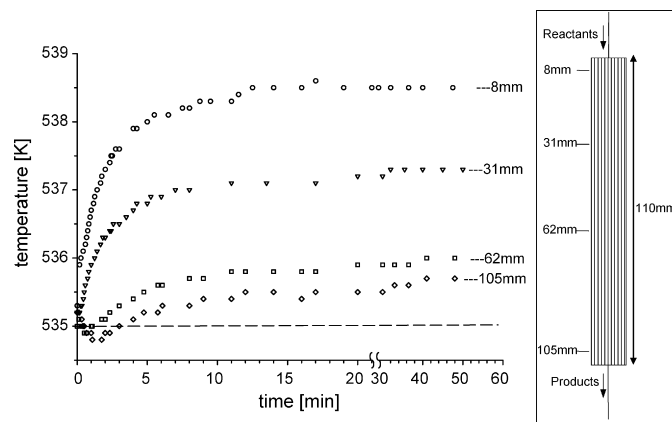


Fig. 11. Temperature variations as function of time during OSRM start-up at different axial positions. Catalyst: CZACr/i; W/F: 3.5 kg<sub>cat</sub>/s/mmol; total flow rate = 100 mL/min.

inlet, the temperature rise is less pronounced, indicating the contribution of the endothermic steam-reforming. In the middle and end of the reactor (62 and 105 mm), a temperature drop is observed over the first two minutes, followed by a rise up to the steady state. This temporary temperature decrease can be explained by a simultaneous endothermic reaction and a lack of energy supply from the methanol oxidation. But after 20 min, a stationary axial temperature profile is established with a small hot-spot of 3.5 K at 8 mm from the reactor entrance.

##### 4.4.2. Thermal axial profile

Stationary axial temperature profiles were measured in the reactor center for different reaction conditions (see Table 3). An example is given in Fig. 12 where the maximum temperature rise of 3.3 K is near the reactor entrance. At longer distances the temperature decreases and reaches asymptotically the wall temperature. Due to the high thermal conductivity of the catalytic brass-wires ( $\lambda = 118$  W/(m K)) the energy produced by fast methanol oxidation is efficiently transferred to the reactor center and exit, where the endothermic steam-reforming takes place. Compared to the nearly isothermal behavior of the string reactor, a pronounced temperature gradient was observed in a conventional fixed bed reactor. The latter was packed by a commercial Cu/Al<sub>2</sub>O<sub>3</sub> with a particle diameter of 0.48 mm,

Table 3

Characteristics of OSRM in the string reactor and in the fixed-bed reactor (methanol 16.5 vol.%, water 16.5 vol.%, oxygen 2 vol.% in Ar; total flow rate 100 mL (STP)/min)

	String reactor	Fixed-bed reactor
Catalyst	CZACr/i	Cu/Al <sub>2</sub> O <sub>3</sub>
T <sub>0</sub> (K)	535	481
W/F (kg <sub>cat</sub> /s/mmol)	3.5	0.06
Void fraction	0.33	0.50
X(CH <sub>3</sub> OH)	0.43	0.43
S(CO)	0.009	0.036

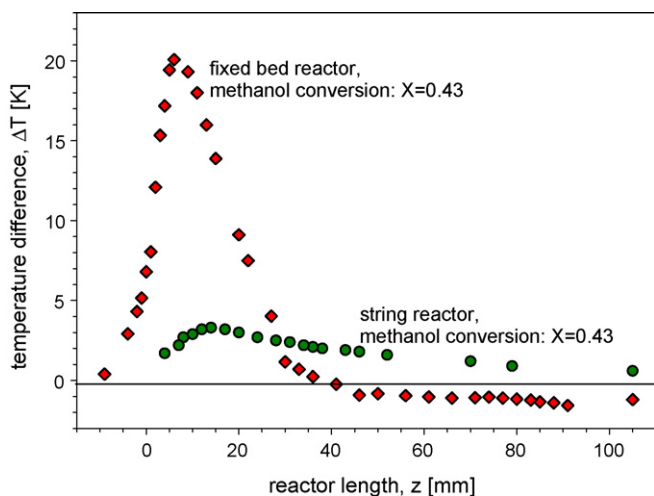


Fig. 12. Temperature axial profile during OSRM reaction at a methanol conversion of 43%. Catalyst: CZACr/i; W/F = 3.5 kg<sub>cat</sub> s/mm<sup>3</sup>; total flow rate = 100 mL/min.

which corresponds to the diameter of the brass wires used for the string reactor. The catalyst particles were diluted with quartz beads in order to compare the temperature profile with the one in the string reactor at the same conversion and on the same reactor length. The characteristics of the fixed bed compared to the string reactor are summarized in Table 3. The measured profiles are shown in Fig. 12. At the entrance of the reactor, the temperature increases drastically giving a hot-spot of 20 K at a 7 mm distance, whereas in the second part of the reactor the temperature is 2 K below the wall temperature (cold-spot).

**4.4.2.1. Influence of methanol conversion.** The effect of methanol conversion on thermal axial profile was studied by varying the reactor wall temperature. Fig. 13 illustrates the measured profiles for three different reactor temperatures: 525,

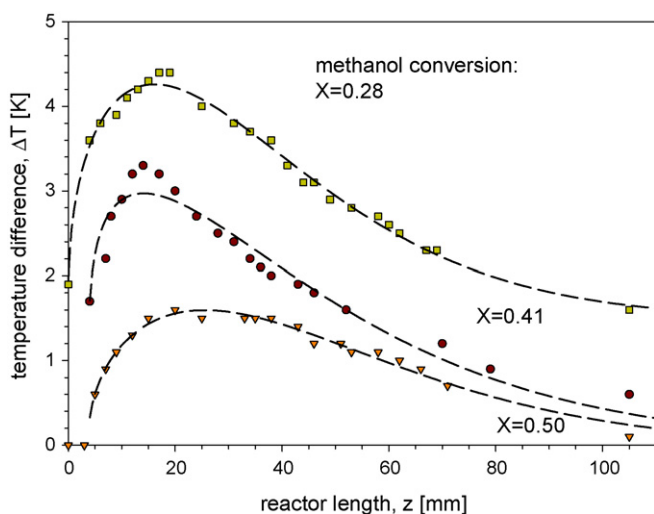


Fig. 13. Temperature axial profiles during OSRM reaction at three different methanol conversions. Catalyst: CZACr/i; W/F = 3.5 kg<sub>cat</sub> s/mm<sup>3</sup>; total flow rate = 100 mL/min.

535 and 550 K corresponding to methanol conversions of 28, 43 and 50%, respectively. With increasing methanol conversion, the temperature profile becomes more flat due to the increased energy consumption by steam-reforming. As methanol oxidation is fast compared to reforming, the two reactions can be considered as being consecutive. With the methanol/oxygen ratio of  $a = 0.12$ , complete oxygen consumption corresponds to 8% of methanol conversion. Higher methanol conversions indicate a contribution of the steam-reforming. Methanol conversion can also be influenced by changing the contact time at constant temperature. The observed temperature profiles show the same tendency: they become flatter with increasing conversion and the hot-spot disappeared for conversions >75% [48].

## 5. Conclusions

Thermal coupling of methanol steam-reforming and its oxidation was performed by carrying out the oxidative steam-reforming of methanol in a compact string reactor with catalytic brass wires. This allows hydrogen production in autothermal mode. The string reactor presents micro-channels for the reacting gases between the wires placed in parallel into a tube and showing hydrodynamics similar to multi-channel micro-reactors. The catalytic wires were prepared by Al-alloy formation on the surface of brass wires followed by partial leaching of Al in basic solution. The catalyst presents a porous layer with the morphology of Raney metals and the chemical composition consistent with the Cu/Zn/Al-mixed oxide. The catalyst surface was additionally modified by incorporating chromium leading to Cr/Cu-spinel. This decreases the degree of the reduction of copper oxide and its sintering leading to a stable catalyst. The selectivity towards carbon dioxide was 98% for a methanol conversion of 91.5% being higher than predicted for the water–gas shift equilibrium. It was concluded that carbon monoxide is produced from the reverse water–gas shift reaction when methanol has undergone almost complete conversion. Thermal axial profiles showed a difference of 3.5 K along the string reactor. In comparison, in the fixed-bed reactor the temperature change was ~25 K. Therefore, the micro-structured string reactor with brass wires improves heat transfer allowing a close to isothermal performance of OSRM. String reactor presents a short start-up and a fast transient behavior showing a rapid temperature change when adjusting the oxygen amount introduced into the reactor. A further advantage is that the micro-structured string reactor with outer diameters in the centimeter range can be easily integrated in traditional processes.

## Acknowledgements

The financial support from the Swiss National Science Foundation and the Max-Buchner-Forschungsstiftung is gratefully acknowledged. The authors thank Brian Senior and Nicolas Xanthopoulos for collaboration in the catalyst characterization by XPS and SEM.

## References

- [1] L.F. Brown, *Int. J. Hydrogen Energy* 26 (2001) 381.
- [2] K. Ledjeff-Hey, V. Formanski, T. Kalk, J. Roes, *J. Power Sources* 71 (1998) 199.
- [3] J.R. Rostrup-Nielsen, *Phys. Chem. Chem. Phys.* 3 (2001) 283.
- [4] B. Höhlein, M. Boe, J. Bogild-Hansen, P. Bröckererhoff, G. Colman, B. Emonts, R. Menzer, E. Riedel, *J. Power Sources* 61 (1996) 143.
- [5] P. Reuse, A. Renken, K. Haas-Santo, O. Görke, K. Schubert, *Chem. Eng. J.* 101 (2004) 133.
- [6] N. Edwards, S.R. Ellis, J.C. Frost, S.E. Golunski, A.N.J.V. Keulen, N.G. Lindewald, J.G. Reinkingh, *J. Power Sources* 71 (1998) 123.
- [7] K. Geissler, E. Newson, F. Vogel, T.B. Truong, P. Hottinger, A. Wokaun, *Phys. Chem. Chem. Phys.* 3 (2001) 289.
- [8] J. Agrell, H. Birgersson, M. Boutonnet, *J. Power Sources* 106 (2002) 249.
- [9] S. Velu, K. Suzuki, M.P. Kapoor, F. Ohashi, T. Osaki, *Appl. Catal. A: Gen.* 213 (2001) 47.
- [10] K. Geissler, Swiss Federal Institute of Technology, EPF-Lausanne, No. 2442, 2002.
- [11] M. Schuessler, O. Lamla, T. Stefanovski, C. Klein, D. Megede, *Chem. Eng. Technol.* 24 (2001) 1141.
- [12] B. Lindström, J. Agrell, L.J. Pettersson, *Chem. Eng. J.* 93 (2003) 91.
- [13] L. Kiwi-Minsker, O. Wolfrath, A. Renken, *Chem. Eng. Sci.* 57 (2002) 4947.
- [14] O. Wolfrath, Thèse No. 2384, EPFL, 2001.
- [15] C. Horny, L. Kiwi-Minsker, A. Renken, *Chem. Eng. J.* 101 (2004) 3.
- [16] L. Kiwi-Minsker, *CHIMIA* 56 (2002) 159.
- [17] J. Agrell, M. Boutonnet, J.L.G. Fierro, *Appl. Catal. A: Gen.* 253 (2003) 213.
- [18] Y. Choi, H.G. Stenger, *Appl. Catal. B: Environ.* 38 (2002) 259.
- [19] S. Murcia-Mascaros, R.M. Navarro, L. Gomez-Saneiro, U. Constantino, M. Nocchetti, J.L.G. Fierro, *J. Catal.* 198 (2001) 338.
- [20] H.E. Curry-Hyde, M.S. Wainwright, D.J. Young, *Appl. Catal.* 77 (1991) 75.
- [21] J.R. Mellor, N.J. Coville, A.C. Sofianos, R.G. Copperthwaite, *Appl. Catal. A: Gen.* 164 (1997) 185.
- [22] J. Toyir, M. Saito, I. Yamauchi, S. Luo, J. Wu, I. Takahara, M. Takeuchi, *Catal. Today* 45 (1998) 245.
- [23] M.V. Twigg, M.S. Spencer, *Appl. Catal. A: Gen.* 212 (2001) 161.
- [24] Z. Wang, J. Xi, W. Wang, G. Lu, *J. Mol. Catal. A: Chem.* 191 (2003) 123.
- [25] B. Lindström, L.J. Pettersson, *Catal. Lett.* 74 (2001) 27.
- [26] L. Yong-Feng, D. Kin-Fa, L. Wei-Ming, *Int. J. Hydrogen Energy* 29 (2004) 1617.
- [27] I. Melian-Cabrera, M.L. Granados, P. Terreros, J.L.G. Fierro, *Catal. Today* 45 (1998) 251.
- [28] G.R. Sheffer, T.S. King, *J. Catal.* 115 (1989) 376.
- [29] J. Batista, A. Pintar, D. Mandrino, M. Jenko, V. Martin, *Appl. Catal. A: Gen.* 206 (2001) 113.
- [30] L. Alejo, R. Lago, M.A. Pena, J.L.G. Fierro, *Appl. Catal. A: Gen.* 162 (1997) 281.
- [31] J. Agrell, M. Boutonnet, I. Melian-Cabrera, J.L.G. Fierro, *Appl. Catal. A: Gen.* 253 (2003) 201.
- [32] S. Velu, K. Suzuki, C.S. Gopinath, H. Yoshida, T. Hattori, *Phys. Chem. Chem. Phys.* 4 (2002) 1990.
- [33] B. Lindström, L.J. Pettersson, P. Govind Menon, *Appl. Catal. A: Gen.* 234 (2002) 111.
- [34] J.L.G. Fierro, M. Lo Jacono, M. Inversi, P. Porta, F. Cioci, R. Lavecchia, *Appl. Catal. A: Gen.* 137 (1996) 327.
- [35] J.P. Shen, S. Chunshan, *Catal. Today* 77 (2002) 89.
- [36] H. Agaras, G. Cerrella, M.A. Laborde, *Appl. Catal.* 45 (1988) 53.
- [37] E. Santacesaria, S. Carra, *Appl. Catal.* 5 (1983) 345.
- [38] J.C. Amphlett, M.J. Evans, R.F. Mann, R.D. Weir, *Can. J. Chem. Eng.* 63 (1985) 605.
- [39] J.C. Amphlett, R.F. Mann, B.A. Peppley, *Stud. Surf. Sci. Catal.* 81 (1994) 409.
- [40] H. Takahashi, N. Takezawa, H. Kobayashi, *Appl. Catal.* 2 (1982) 363.
- [41] R.C. Reid, J.M. Prausnitz, B.E. Poling, McGraw-Hill International Editions, 1986.
- [42] H. Purnama, T. Ressler, R.E. Jentoft, H. Soerijanto, R. Schlögl, R. Schomäcker, *Appl. Catal. A: Gen.* 259 (2004) 83.
- [43] J.P. Breen, F.C. Meunier, J.R.H. Ross, *Chem. Commun.* (1999) 2247.
- [44] J.P. Breen, J.R.H. Ross, *Catal. Today* 51 (1999) 521.
- [45] C.J. Jiang, D.L. Trimm, M.S. Wainwright, *Appl. Catal. A: Gen.* 93 (1993) 245.
- [46] M.J.L. Ginés, A.J. Marchi, C.R. Apestequia, *Appl. Catal. A: Gen.* 154 (1997) 155.
- [47] J.R. Mellor, N.J. Coville, A.C. Sofianos, R.G. Copperthwaite, *Appl. Catal. A: Gen.* 164 (1997) 171.
- [48] C. Horny, Développement d'un réacteur microstructuré basé sur des filaments métalliques catalytiques, Production autotherme d'hydrogène par steam-reforming oxydatif du méthanol, No. 3271, Ecole polytechnique fédérale de Lausanne, 2005.